SCIENTIFIC REPORTS

OPEN

CONFERENCE PROCEEDINGS

APEnergy2014

SUBJECT AREAS:
NANOSCALE MATERIALS
ELECTROCATALYSIS

Received
30 January 2014

Accepted
27 February 2014

Published
29 August 2014

Correspondence and requests for materials should be addressed to J.C. (chenabc@nankai.edu.cn) or F.Y.C. (fycheng@nankai.edu.cn)

M(Salen)-derived Nitrogen-doped M/C (M = Fe, Co, Ni) Porous Nanocomposites for Electrocatalytic Oxygen Reduction

Jing Du, Fangyi Cheng, Shiwen Wang, Tianran Zhang & Jun Chen

Key Laboratory of Advanced Energy Materials Chemistry (Ministry of Education), Collaborative Innovation Center of Chemical Science and Engineering, Chemistry College, Nankai University, Tianjin 300071, China.

Carbonaceous materials containing non-precious metal and/or doped nitrogen have attracted tremendous attention in the field of electrochemical energy storage and conversion. Herein, we report the synthesis and electrochemical properties of a new family of nitrogen-doped metal/carbon (M/N/C, M = Fe, Co, Ni) nanocomposites. The M/N/C nanocomposites, in which metal nanoparticles are embedded in the highly porous nitrogen-doped carbon matrix, have been synthesized by simply pyrolyzing M(salen) (salen = N,N′-bis(salicylidene)-ethylenediamine) complex precursors. The prepared Co/N/C and Fe/N/C exhibit remarkable electrocatalytic activity (with onset potential of 0.96 V for Fe/N/C and half-wave potential of 0.80 V for Co/N/C) and high stability for the oxygen reduction reaction (ORR). The superior performance of the nanocomposites is attributed to their bimodal-pore structure, high surface area, as well as uniform distribution of high-density nitrogen and metal active sites.

Electrocatalysis of the oxygen reduction reaction (ORR) plays the key role in electrochemical energy storage and conversion technologies such as fuel cells and metal-air batteries[1,2]. To date, noble metals and alloys have been known as the state-of-the-art ORR electrocatalysts[3–7]. Nevertheless, the high cost and scarcity of noble metals prohibit their large-scale practical application and necessitate the development of alternative earth-abundant materials with high electrocatalytic performance and wide availability[8–13]. Porous carbonaceous materials have attracted extensive interest because of their prominent advantages including large surface area, high thermal and chemical stability, and high electrical conductivity[14,15]. However, carbon itself exhibits low intrinsic ORR activity[16,17]. Recent studies have shown that the incorporation of nitrogen heteroatom and nonprecious transition metals into nanostructured carbon materials (e.g., carbon nanotubes and graphene) can greatly improve the electrocatalytic performance[18,19]. Generally, nitrogen-doped carbon materials can be synthesized by two approaches[20,21]: (i) directly doping during the synthesis of carbon materials; (ii) post-treatment of the as-prepared carbon materials with nitrogen precursor. Particularly, nitrogen-doped and metal-contained carbon composites (M/N/C, M = Fe, Co) synthesized via pyrolysis of precursors containing metal salts, nitrogen and macrocyclic compounds have been demonstrated to be active for catalyzing ORR[22–31]. However, the synthesis of these composites often involves pyrolysis at high temperature and carbonization in NH_3 atmosphere, which induce severe loss of carbon mass, reduce density of active sites, and shorten the lifespan of these catalysts[30–33]. Furthermore, the ORR properties of the synthesized M/N/C composites depend greatly on the nature of the metal-containing macrocyclic precursors, which affect the particle size, texture, metal and/or nitrogen content, and carbonaceous structures[21,29,34,35]. To prepare cheap and efficient M/N/C catalysts, it is desirable to exploit a low-cost precursor that can be easily converted to high-surface-area porous carbon matrix integrating high-loading of metal and nitrogen.

In this study, we reported a facile synthesis of M/N/C porous nanocomposite catalysts from a family of simple organic precursors, M(salen) (M = Co, Fe, Ni; salen = N,N′-bis(salicylidene)-ethylenediamine) complexes. These inexpensive complexes can be easily synthesized and contain abundant nitrogen sites for coordination with transition metals. Recently, we showed that carbonizing Sn(salen) resulted in ultrasmall Sn nanoparticles embedded in N-doped porous carbon network, which exhibited excellent electrochemical performance for Li-ion batteries[36]. Herein, we demonstrate that M(salen) (M = Co, Fe, Ni) can be carbonized at relatively low

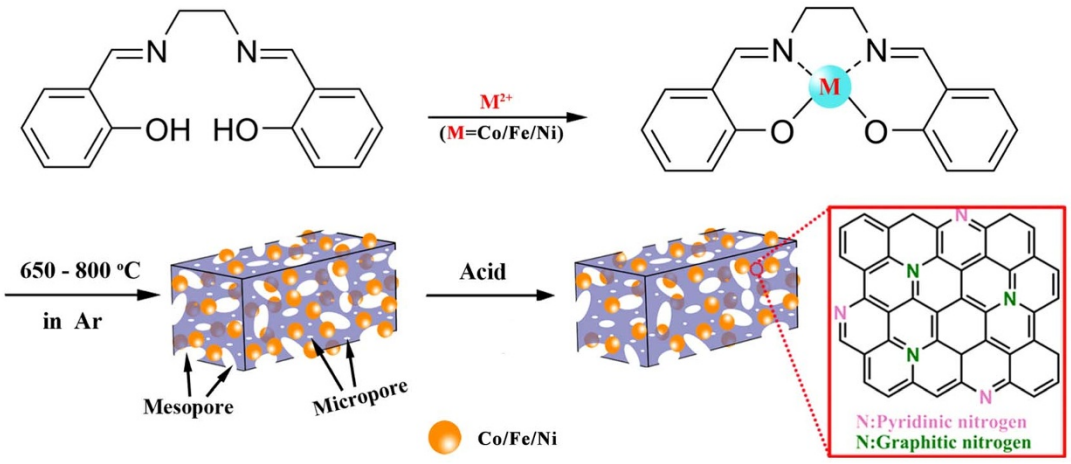

Figure 1 | **Schematic illustration of the preparation of M/N/C (M = Co, Fe, Ni) porous nanocomposite catalysts.**

temperatures to form in situ nitrogen-doped and metal-included carbon composites without post treatment in NH_3 atmosphere. Moreover, direct pyrolysis of the simple complex precursors generates simultaneously well-defined micropores and mesopores, which could enhance the exposure of the ORR active sites and mass transport. Remarkably, the as-prepared M/N/C nanocomposites are featured with homogeneous distribution of small metal nanoparticles, high specific surface areas, and relatively high content of doped nitrogen. As ORR catalysts in alkaline electrolytes, the nanocomposites exhibit comparable activity and superior durability to the benchmark Pt/C.

Results and discussion

Material preparation and characterizations. Figure 1 illustrates the synthesis processes of M/N/C (M = Co, Fe, Ni) nanocomposite catalysts. First, M(salen) precursors were synthesized by directly reacting H_2(salen) with the corresponding metal nitrates. Second, the obtained precursor was subjected to heat treatments under an Ar atmosphere. The pyrolysis temperature was selected by referencing to the thermogravimetric curves of the precursor M(salen) complexes (additional information, Figure S1). Subsequently, the heat-treated solid powders were leached in acid to remove unstable and inactive species. The acid-washed samples were annealed in Ar for further graphitization. For comparison, we prepared metal-free catalyst (H/N/C) with similar procedures by pyrolyzing H_2(salen).

Figure 2 shows the representative transmission electron microscopy (TEM) and scanning electron microscopy (SEM) imaging of Co/N/C, Fe/N/C and Ni/N/C synthesized at pyrolysis temperature of 700°C. As shown in TEM images (Figures 2a, d, and g), Co, Fe or Ni nanoparticles (black dots) with uniform particle size are

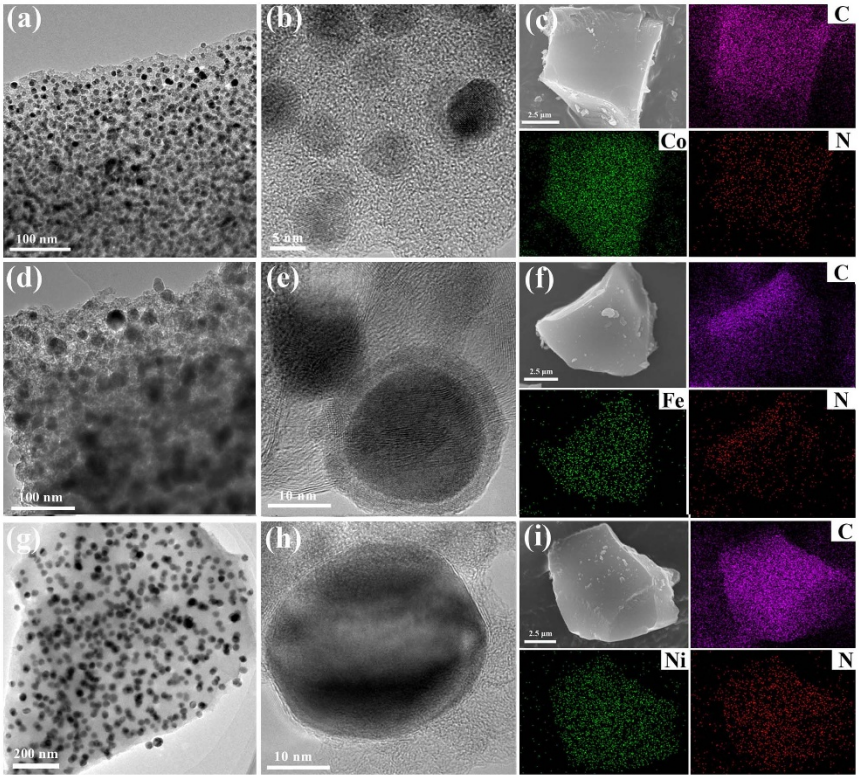

Figure 2 | **SEM and TEM images of (a–c) Co/N/C, (d–f) Fe/N/C, and (g–i) Ni/N/C catalysts: (a,b,d,e,g,h) TEM images; (c,f,i) SEM images and the corresponding EDS mapping.**

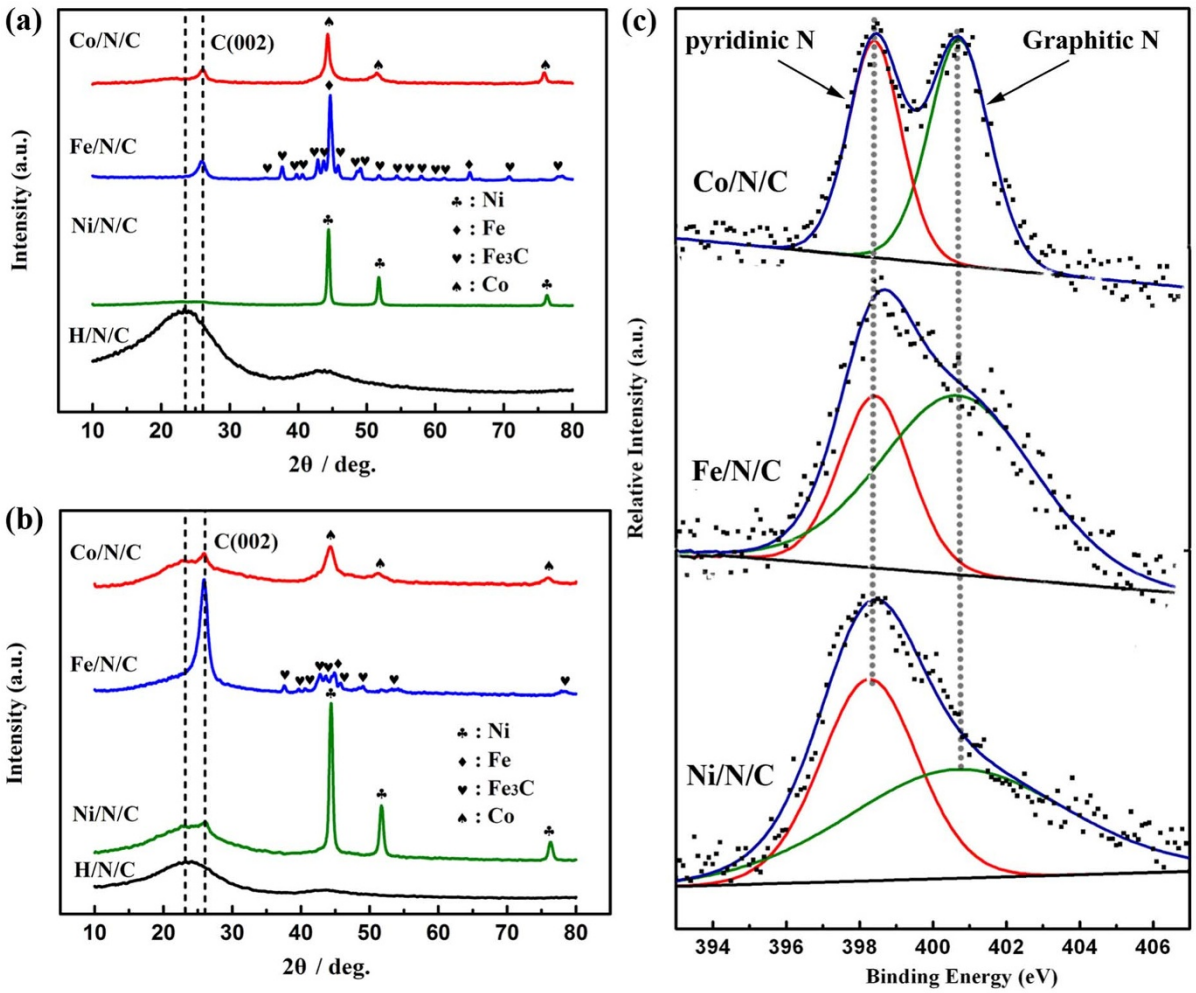

Figure 3 | XRD patterns of Co/N/C, Fe/N/C, Ni/N/C and H/N/C catalysts (a) before and (b) after acid leaching and post annealing. (c) N 1s XPS spectra showing the presence of pyridinic and graphitic N.

homogenously embedded in the nitrogen doped carbon framework (gray matrix). From high-magnification TEM images (Figures 2b, e, and h), the typical sizes of metal nanoparticles in Co/N/C, Fe/N/C and Ni/N/C are 6–7, 20–40 and 20–30 nm, respectively. Among the three nanocomposites, Fe/N/C has relatively larger average particle size and contains onion-like graphitic carbon nanostructure (Figure 2e). The high graphitization degree of carbon can be attributed to the prominent catalytic ability of Fe towards carbonization[22,37]. Typically, the obtained samples present irregular particulate shape with size of a few micrometers; while carbon, metal (Co, Fe or Ni), and nitrogen are homogeneously distributed within the carbon matrix (Figures 2c, f, and i). It should be noted that the nanoparticles grow and agglomerate as the pyrolysis temperature increases higher than 700°C (Figure S2).

Thermogravimetric analysis (Figure S3) was performed to analyze the content of metal in the M/N/C (M = Co, Fe, Ni) catalysts. The metal content in the nanocomposites was determined to be 25.8, 10.2, and 19.1 wt.% for Co/N/C, Fe/N/C, and Ni/N/C, respectively. Figure 3a shows the X-ray diffraction (XRD) pattern of H_2(salen) and M/N/C (M = Co, Fe, Ni) samples pyrolyzed at 700°C before acid leaching. The wide and weak diffraction peaks at 2θ of 26.3° are ascribed to the (002) plane of carbon. Relatively higher peak intensity of Co/N/C and Fe/N/C indicates a higher graphitization degree. Crystalline metallic phases of Co, Fe and Ni can be found in the nanocomposites. However, an additional Fe_3C phase is detected in the Fe/N/C sample. The formation of Fe_3C can be predicted from the phase diagram, while other metal carbides such as Fe_2C, Co_3C and Ni_3C are metastable at 700°C and thus are not observed in the pyrolyzed product[38–40]. After acid leaching and annealing, the diffraction peaks indexed to carbon become much stronger (Figure 3b), suggesting enhanced graphitization of the nitrogen doped nanocomposites. Notably, most of Fe is etched by acid leaching of Fe/N/C, leaving the presence of iron carbide. In contrast to M/N/C catalysts, H/N/C shows the presence of disordered carbon in the XRD pattern. This comparison suggests that transition metal can catalyze the graphitization[37]. Furthermore, a series of Co/N/C samples were prepared at varied pyrolysis temperatures (Figure S2, S4). A higher temperature favors the formation of crystalline carbon but leads to the increase of particle size.

Nitrogen can be viewed as a n-type dopant that donates electrons to carbon, which can facilitate the electronic conductivity and ORR activity[41]. X-ray photoelectron spectroscopy (XPS) provides evidence for the incorporation of nitrogen into the carbon matrix during annealing. As shown in Figure 3c, XPS N 1s spectra of all M/N/C catalysts can be fitted with two deconvoluted peaks that are assignable to the pyridinic (398.8 eV) and graphitic (401.1 eV) nitrogen. Generally, pyridinic and graphitic N atoms are considered as possible active sites to participate in the ORR electrocatalysis[29,42]. From XPS analysis, the nitrogen content in the nanocomposites was determined to be 6.53, 4.02, and 3.16 wt.% for Co/N/C, Fe/N/C, and Ni/N/C, respectively, which agreed with the values from elemental analysis. Besides N, signal of oxygen can be also found in the XPS spectra (Figure S5). The oxygen content of the synthesized catalysts is 4.32, 4.30, and 3.45 wt.% for Co/N/C, Fe/N/C, and Ni/N/C, respectively.

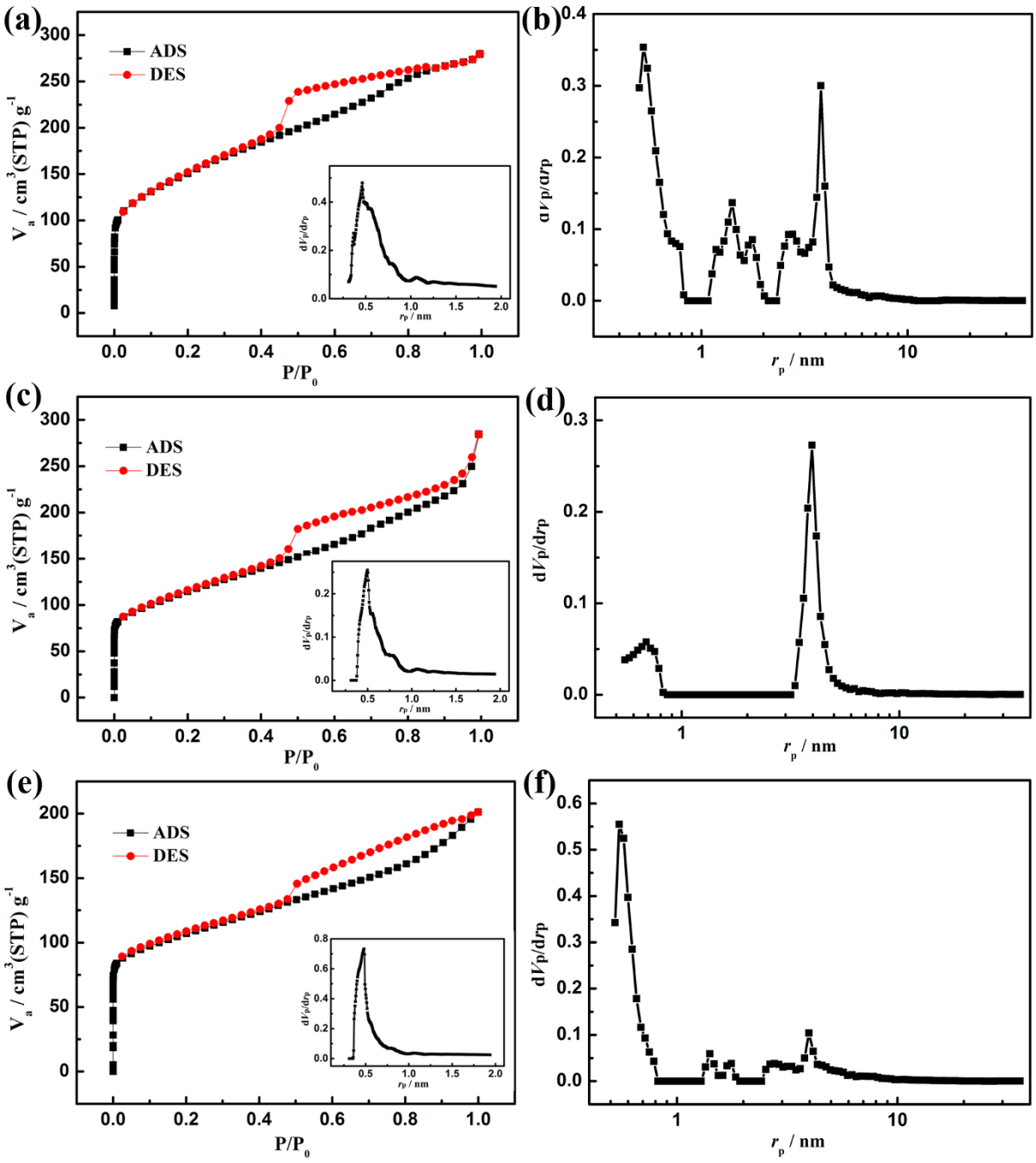

Figure 4 | (a,c,e) Nitrogen adsorption/desorption isotherms and (b,d,f) pore size distribution (PSD) of Co/N/C (a,b), Fe/N/C (c,d), and Ni/N/C (e,f). Insets of (a,c,e) show the PSD determined from the Horvath-Kawazoe (HK) method while results in (b,d,f) are based on the Density Functional Theory (DFT) method.

Possibly, the presence of oxygen in the composites can be attributed to the following factors: residual oxygen-containing species from the precursors, oxidation of metal nanoparticles, and adsorbed oxygen on the surface or in the pores. It is reported that N and O species co-present as dopants in the carbon structure could contribute to the electrocatalytic activity towards the ORR due to synergistic effect[15].

Nitrogen adsorption/desorption isotherms were performed to characterize the texture of the synthesized M/N/C nanocomposites. All isotherms (Figures 4a, c, and e) display the combination of typical IUPAC type-I and type-IV adsorption/desorption behaviors. The steep increase of N_2 uptake at low pressure and hysteresis loop at high pressure are characteristics of meso- and micro-porous structures. The determined Brunauer-Emmett-Teller (BET) specific surface areas of Co/N/C, Fe/N/C and Ni/N/C nanocomposites are 523, 483, and 350 $m^2\ g^{-1}$, respectively. The corresponding pore size distribution (PSD) of micropores (inset of Figures 4a, c, and e) is centered at 0.46, 0.50, and 0.49 nm, according to the Horvath-Kawazoe (HK) model. Analysis based on the Density Functional Theory (DFT) model (Figures 4b, d, and f) gives more PSD information at both micropore and mesopore scale. The mesopore size distribution is centered at 3.80, 3.96, and 3.95 nm for Co/N/C, Fe/N/C and Ni/N/C, respectively. Although having similar average micropore size, the three nanocomposites show different PSD profiles. While bimodal size distribution is observed in all samples, the proportion of mesopores to micropores differs much from each other. The results indicate that the texture (i.e., surface area and porous

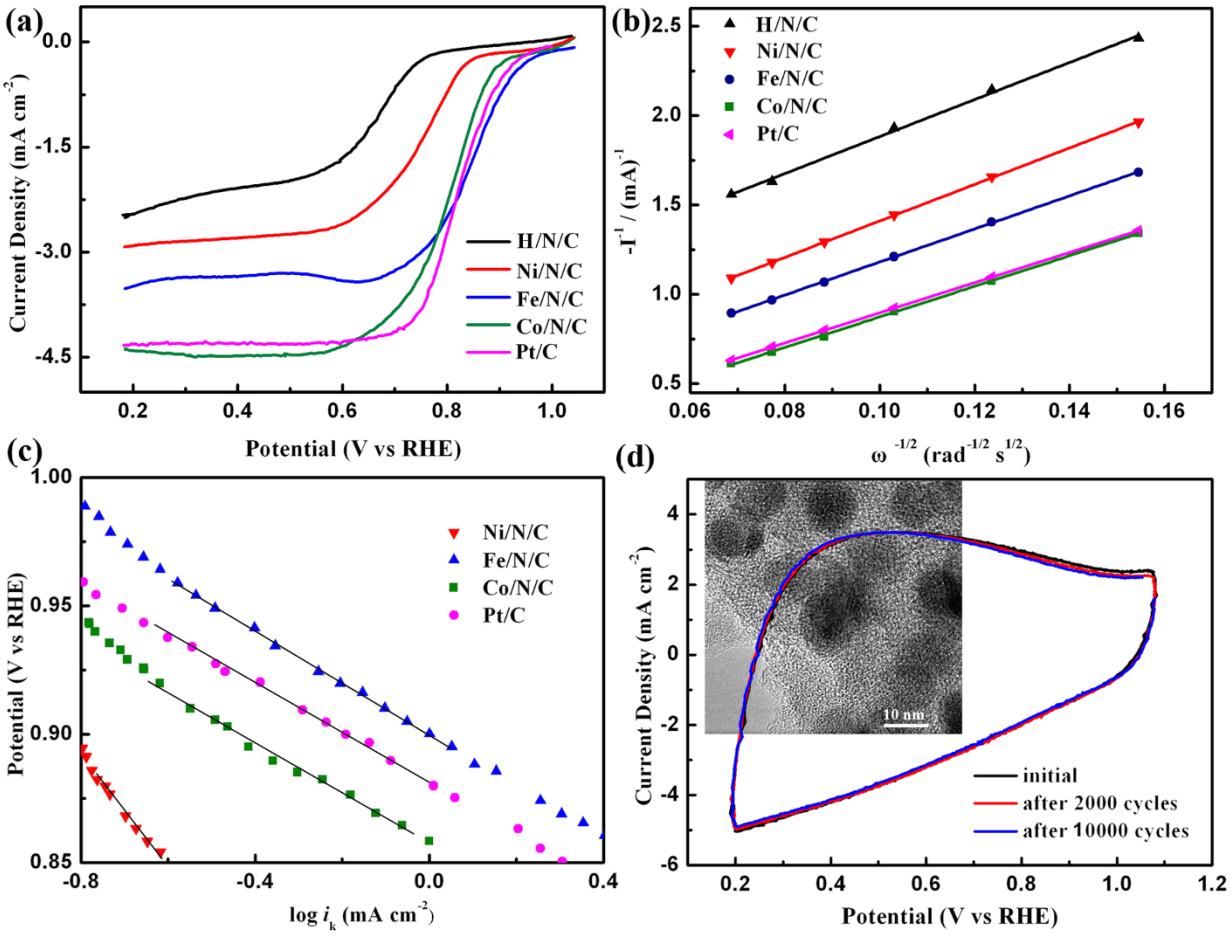

Figure 5 | (a) ORR polarization curves of Co/N/C, Fe/N/C, Ni/N/C, H/N/C, and commercial Pt/C. (b) Koutecky-Levich plots of different catalysts at 0.5 V. (c) Tafel plots. (d) Typical cyclic voltammograms of Co/N/C, inset showing the TEM image after 10000 cycles.

structure) of M/N/C depends greatly on the nature of the M(salen) precursors. The presence of Co and Fe results in higher surface areas and benefits the formation of mesopores.

Electrocatalytic properties. The metal-in-N-doped-carbon nanostructure, high surface area, and bimodal porous character of the synthesized M/N/C composites motivated us to investigate their electrocatalytic properties towards the ORR (experimental details are described in methods). At first, we tested Co/N/C samples synthesized at varied pyrolysis temperatures (650–800°C) and found that the best performance was realized at 700°C (Figure S6). This is possibly due to a balance of active site density, particle size, surface area, and electron conductivity in the nanocomposite[29,43]. Then, the ORR activities of M/N/C nanocomposites synthesized at 700°C were detailedly evaluated using rotating-disk electrode (RDE) measurements (Figure S7).

Figure 5a displays the typical ORR polarization curves at rotating rate of 900 rpm (round per minute). Compared to the metal-free H/N/C sample, the three M/N/C (M = Co, Fe, Ni) catalysts exhibit higher activity, in terms of higher onset and half-wave potentials. Among the nanocomposites, Co/N/C and Fe/N/C are more active. Remarkably, Fe/N/C gives a more positive onset potential than that of the benchmark commercial Pt/C. The half-wave potential of Co/N/C is 0.80 V, which is only 25 mV lower than that of Pt/C and is among the best results reported for nonprecious catalysts[30,44]. Notably, Co/N/C shows a higher limiting current density (based on the geometric area of the electrode) relative to Fe/N/C. This different current may be attributed to the difference in factors such as particle size, surface area, and metal/nitrogen/oxygen content. For comparison, we also calculated the mass activities (MA) with respect to the mass of metal (Figure S8). Again, Co/N/C and Fe/N/C possess higher MA values compared with Ni/N/C. In particular, Fe/N/C slightly outperforms Pt/C in mass activity. The determined MA of Pt/C is comparable to literature result[45], which validates our present investigation and confirms the prominent activity of Co/N/C and Fe/N/C.

The ORR kinetics was also studied by Koutecky-Levich (K-L)[46,47] determination (Figure 5b and Figure S7). The K-L curves are constructed according to the following K-L equation:

$$\frac{1}{i} = \frac{1}{i_k} + \frac{1}{i_d} = \frac{1}{nFAkC^0} - \frac{1}{0.62nFAD_{O_2}^{\frac{2}{3}}\upsilon^{-\frac{1}{6}}C^0\omega^{\frac{1}{2}}} \qquad (1)$$

where i, i_k, and i_d corresponds respectively to the measured, kinetic, and diffusion-limiting current, n is the overall transferred electron number, F is the Faraday constant, A is the geometric electrode area (cm^2), k is the rate constant for oxygen reduction, C^0 is the saturated concentration of oxygen in 0.1 M KOH, D_{O2} is the diffusion coefficient of oxygen, υ is the kinetic viscosity of solution, and ω is the rotation rate (rads^{-1})[46]. The K-L plots exhibit good linearity at potentials ranging from 0.3 to 0.6 V. At 0.5 V, the transferred number (n) of electrons on Co/N/C, Fe/N/C and Ni/N/C catalysts was calculated to be 4.10, 3.96 and 3.60, respectively. Thus, the ORR on these nanocomposites followed the apparent four-electron transfer pathway. In Tafel plots (Figure 5c), Co/N/C, Fe/N/C and Pt/C catalysts display very similar slope and close kinetic current densities, especially in the low overpotential region. This again verifies the superior ORR catalytic properties of Co/N/C and Fe/N/C. The high activity of the

nanocomposites is ascribed to high density of active sites and favorable mass-transport properties, as a result of the bimodal porous structures and evenly distributed metal nanoparticles, nitrogen and oxygen species in the carbon matrix[29,34]. It is well known that micropores are beneficial to diffusion of O_2 gas while mesopores are helpful to smooth transportation of electrolyte and prevent unwanted agglomeration of active sites[48], which contribute to enhanced electrocatalysis.

Besides high activity, the M/N/C nanocomposites exhibit respectable durability. Figure 5d and Figure S9 show the cyclic voltammograms (CVs) of the nanocomposites and the comparative Pt/C electrode up to 10000 continuous cycles. The decay of current on Co/N/C is negligible upon the extended cycling, indicating excellent durability in alkaline solution. The catalytic stability of Co/N/C is much better than that of commercial Pt/C. It is noted that the dispersion and particle size of metal nanoparticles in Co/N/C were well retained after long-term stability test, as demonstrated by the TEM images (see comparison in Figure 2b and 5d inset). The excellent electrocatalytic stability can be attributed to the novel porous nanostructures that anchor the homogenously distributed small nanoparticles. This structure is advantageous over the case of carbon supported Pt nanoparticles, which tend to aggregate or detach from the substrate during prolonged electrochemistry process[49].

In summary, we have developed a facile method to prepare a new family of M/N/C (M = Co, Fe, Ni) porous nanocomposite by pyrolyzing M(salen) complexes. Furthermore, the synthesized composites exhibit high ORR activity (i.e., low overpotential and large current density) and remarkable electrochemical stability in alkaline electrolyte. The prominent performance is associated with beneficial factors including small metal particle size, high surface area and nanoporous structure, as well as uniformly-distributed and high-density of active sites in the carbon matrix. Our results indicate that transition metal salen compounds are promising cheap precursors for the design and synthesis of nitrogen-doped and metal-incorporated carbon nanocomposite catalysts, which should find potential applications in diverse electrochemical energy storage and conversion devices.

Methods

General materials. N,N′-bis(salicylidene)-ethylenediamin (salen), ferrous nitrate, nickel nitrate, cobalt nitrate, isopropanol (99.5%), ethanol (99.9%) and Nafion (5%) were all purchased from Sigma-Aldrich. Vulcan XC-72 carbon and carbon supported Pt nanoparticles (Pt/C, 20 wt.% Pt) were supplied by Johnson Matthey Company.

Synthesis of M(salen). In a typical synthesis of Ni(salen), 3.5 g (13 mmol) of salen was dissolved in 30 mL of absolute alcohol in a three-necked, round-bottom flask. Subsequently, 20 mL 0.6 M nickel nitrate ethanol solution was dripped and refluxed for 1 h at 65°C. After cooling, solid precipitates were filtered, washed and vacuum-dried at 80°C. Following similar procedures, Co(salen) and Fe(salen) were synthesized by using Co and Fe nitrates.

Catalyst preparation. The M/N/C (M = Co, Fe, Ni) catalysts were synthesized as follows: Firstly, M(salen) was pyrolyzed at temperatures ranged from 650–800°C in a cylindrical electric furnace under a flow of Ar gas for 1 h. Then, the resultant sample was leached in 0.5 M H_2SO_4 at 80°C for 8 h to remove unstable species and was washed with de-ionized water. Finally, the catalyst was heat-treated again in an Ar atmosphere for 1 h at the same temperature. Metal-free catalyst was prepared by pyrolyzing H_2(salen) via similar procedures.

Material characterization. XRD was recorded on a Rigaku Mini Flex 600 powder diffractometer (Cu Kα radiation, λ = 1.5406 Å). SEM images were taken on a JEOL JSM-7500F microscope operated at 5 kV. TEM imaging was obtained on Philips Tecnai F20 system operated at 200 kV. Thermogravimetric analysis (TGA) was carried out on a NETZSCH STA 449F3 using a heating rate of 5°C min^{-1} in air or Ar stream. X-ray photoelectron spectroscopy (XPS) data were collected using a Versa Probe PHI 5000 system. Elemental analysis was measured by a vario ELCUBE. Nitrogen adsorption-desorption measurements were performed on Quantachrome Autosorb iQ2.

Electrochemical tests. Electrocatalytic measurements were carried out using a computer-controlled workstation bipotentiostats (AFCBP1, Pine Instrument) assembled with a modulated speed rotator (PHYCHEMI) in a standard three-electrode system at room temperature. Saturated calomel electrode (SCE) and Pt wire served as the reference and counter electrode, respectively. The working electrode was a glassy carbon electrode coated with a thin layer of catalyst. The catalyst ink was prepared by ultrasonically mixing 10.0 mg of as-prepared catalyst with 80 μL of Nafion solution and 450 μL of water/ethanol (1 : 1 v/v) mixed solvent for 30 min to form a homogeneous suspension. A 6.0 μL of the prepared ink was transferred to the surface of a rotation disk electrode (RDE) using microsyringe. The catalyst-afforded electrode was allowed to drying at room temperature. Catalyst loading was approximately 0.458 mg cm^{-2} on the RDE. For comparison, catalytic performance of the benchmark Pt/C (20 wt.% Pt) was also investigated under the same condition.

Cyclic voltammetry and linear sweep voltammetry measurements were carried out in 0.1 M aqueous KOH solution. High-purity oxygen gas was bubbled for 30 min before each test. The required atmosphere was held above the electrolyte throughout the measurements. Unless otherwise stated, all potentials in the text were reported with reference to the reversible hydrogen electrode (RHE) potential scale. In 0.1 M KOH solution, the potential of SCE was calibrated as +0.990 V with respect to RHE. Voltammograms were collected from 0.1 to −0.8 V (*vs.* SCE) under a scanning rate of 5 mV s^{-1} at 400, 625, 900, 1225, 1600, and 2025 rpm.

1. Gasteiger, H. A. & Marković, N. M. Just a dream-or future reality? *Science* **324**, 48–49 (2009).
2. Wu, G. & Zelenay, P. Nanostructured nonprecious metal catalysts for oxygen reduction reaction. *Acc. Chem. Res.* **46**, 1878–1889 (2013).
3. Debe, M. K. Electrocatalyst approaches and challenges for automotive fuel cells. *Nature* **486**, 43–51 (2012).
4. Wang, C., Daimon, H. & Sun, S. H. Dumbbell-like Pt−Fe_3O_4 nanoparticles and their enhanced catalysis for oxygen reduction reaction. *Nano Lett.* **4**, 1493–1496 (2009).
5. Cheng, F. Y. & Chen, J. Metal-air batteries: from oxygen reduction electrochemistry to cathode catalysts. *Chem. Soc. Rev.* **41**, 2172–2192 (2012).
6. Liu, G. C. K. *et al.* Oxygen reduction activity of dealloyed $Pt_{1-x}Ni_x$ catalysts. *J. Electrochem. Soc.* **158**, B919–B926 (2011).
7. Chen, Z. W., Higgins, D., Yu, A., Zhang, L. & Zhang, J. J. A review on non-precious metal electrocatalysts for PEM fuel cells. *Energy Environ. Sci.* **4**, 3167–3192 (2011).
8. Zhao, Z. G. *et al.* In-situ formation of cobalt-phosphate oxygen-evolving complex-anchored reduced graphene oxide nanosheets for oxygen reduction reaction. *Sci. Rep.* **3**, 2263; doi:10.1038/srep02263 (2013).
9. Liang, J., Du, X., Gibson, C., Du, X. W. & Qiao, S. Z. N-doped graphene natively grown on hierarchical ordered porous carbon for enhanced oxygen reduction. *Adv. Mater.* **25**, 6226–6231 (2013).
10. Liang, Y. Y. *et al.* Co_3O_4 nanocrystals on graphene as a synergistic catalyst for oxygen reduction reaction. *Nat. Mater.* **10**, 780–786 (2011).
11. Cheng, F. Y., Su, Y., Liang, J., Tao, Z. L. & Chen, J. MnO_2-based nanostructures as catalysts for electrochemical oxygen reduction in alkaline media. *Chem. Mater.* **22**, 898–905 (2010).
12. Cheng, F. Y. *et al.* Enhancing electrocatalytic oxygen reduction on MnO_2 with vacancies. *Angew. Chem. Int. Ed.* **52**, 2474–2477 (2013).
13. Zhang, Y. W. *et al.* Manageable N-doped graphene for high performance oxygen reduction reaction. *Sci. Rep.* **3**, 2771; doi:10.1038/srep02771 (2013).
14. Liu, X. H. *et al.* Hollow, spherical nitrogen-rich porous carbon shells obtained from a porous organic framework for the supercapacitor. *ACS Appl. Mater. Interf.* **5**, 10280–10287 (2013).
15. Silva, R., Voiry, D., Chhowalla, M. & Asefa, T. Efficient metal-free electrocatalysts for oxygen reduction: polyaniline-derived N- and O-doped mesoporous carbons. *J. Am. Chem. Soc.* **135**, 7823–7826 (2013).
16. Shao, Y. Y., Sui, J. H., Yin, G. P. & Gao, Y. Z. Nitrogen-doped carbon nanostructures and their composites as catalytic materials for proton exchange membrane fuel cell. *Appl. Catal. B* **79**, 89–99 (2008).
17. Wang, H., Cote, R., Faubert, G., Guay, D. & Dodelet, J. P. Effect of the pre-treatment of carbon black supports on the activity of Fe-based electrocatalysts for the reduction of oxygen. *J. Phys. Chem. B* **103**, 2042–2049 (1999).
18. Gong, K. P., Du, F., Xia, Z. H., Durstock, M. & Dai, L. M. Nitrogen-doped carbon nanotube arrays with high electrocatalytic activity for oxygen reduction. *Science* **323**, 760–764 (2009).
19. Chen, P., Xiao, T. Y., Qian, Y. H., Li, S. S. & Yu, S. H. A nitrogen-doped graphene/carbon nanotube nanocomposite with synergistically enhanced electrochemical activity. *Adv. Mater.* **23**, 3192–3196 (2013).
20. Ewels, C. & Glerup, M. Nitrogen doping in carbon nanotubes. *J. Nanosci. Nanotechnol.* **5**, 1345–1363 (2005).
21. Zhang, P. *et al.* ZIF-derived in situ nitrogen-doped porous carbons as efficient metal-free electrocatalysts for oxygen reduction reaction. *Energy Environ. Sci.* **7**, 442–450 (2014).
22. Wu, G., More, K. L., Johnston, C. M. & Zelenay, P. High-performance electrocatalysts for oxygen reduction derived from polyaniline, iron, and cobalt. *Science* **332**, 443–447 (2011).
23. Zhao, Y. *et al.* Can boron and nitrogen codoping improve oxygen reduction reaction activity of carbon nanotubes? *J. Am. Chem. Soc.* **135**, 1201–1204 (2013).
24. Li, Y. *et al.* An oxygen reduction electrocatalyst based on carbon nanotube–graphene complexes. *Nat. Nanotechnol.* **7**, 394–400 (2012).
25. Cheon, J. Y. *et al.* Ordered mesoporous porphyrinic carbons with very high electrocatalytic activity for the oxygen reduction reaction. *Sci. Rep.* **3**, 2715; doi:10.1038/srep02715 (2013).

26. Zhao, Y., Watanabe, K. & Hashimoto, K. Self-supporting oxygen reduction electrocatalysts made from a nitrogen-rich network polymer. *J. Am. Chem. Soc.* **134**, 19528–19531 (2012).
27. Lefevre, M., Proietti, E., Jaouen, F. & Dodelet, J. P. Iron-based catalysts with improved oxygen reduction activity in polymer electrolyte fuel cells. *Science* **324**, 71–74 (2009).
28. Peng, H. *et al*. High performance Fe- and N- doped carbon catalyst with graphene structure for oxygen reduction. *Sci. Rep.* **3**, 1765; doi:10.1038/srep01765 (2013).
29. Liang, H. W., Wei, W., Wu, Z. S., Feng, X. L. & Müllen, K. Mesoporous metal–nitrogen–doped carbon electrocatalysts for highly efficient oxygen reduction Reaction. *J. Am. Chem. Soc.* **135**, 16002–16005 (2013).
30. Parvez, K. *et al*. Nitrogen-doped graphene and its iron-based composite as efficient electrocatalysts for oxygen reduction reaction. *ACS Nano* **6**, 9541–9550 (2012).
31. Byon, H. R., Suntivich, J. & Yang, S. H. Graphene-based non-noble-metal catalysts for oxygen reduction reaction in acid. *Chem. Mater.* **23**, 3421–3428 (2011).
32. Jaouen, F., Lefevre, M., Dodelet, J. P. & Cai, M. Heat-treated Fe/N/C catalysts for O_2 electroreduction: are active sites hosted in micropores? *J. Phys. Chem. B* **110**, 5553–5558 (2006).
33. Charreteur, F., Jaouen, F. & Dodelet, J. P. Iron porphyrin-based cathode catalysts for PEM fuel cells: Influence of pyrolysis gas on activity and stability. *Electrochim. Acta* **54**, 6622–6630 (2009).
34. Lee, J. S., Park, G. S., Kim, S. T., Liu, M. & Cho, J. A highly efficient electrocatalyst for the oxygen reduction reaction: N-doped ketjenblack incorporated into Fe/Fe_3C-functionalized melamine foam. *Angew. Chem. Int. Ed.* **52**, 1026–1030 (2013).
35. Zhu, H., Yin, J., Wang, X. L., Wang, H. Y. & Yang, X. R. Microorganism-derived heteroatom-doped carbon materials for oxygen reduction and supercapacitors. *Adv. Funct. Mater.* **23**, 1305–1312 (2013).
36. Zhu, Z. Q. *et al*. Ultrasmall Sn nanoparticles embedded in nitrogen-doped porous carbon as high-performance anode for lithium-ion batteries. *Nano Lett.* **14**, 153–157 (2014).
37. Zhao, M. *et al*. Effect of transition metal addition on the transformation of carbon black to hollow onion-like nanostructural carbon. *J. Inorg. Mater.* **22**, 599–603 (2007).
38. Easton, E. B. *et al*. Thermal evolution of the structure and activity of magnetron-sputtered TM–C–N (TM = Fe, Co) oxygen reduction catalysts. *Electrochem. Solid-State Lett.* **10**, B6–B10 (2007).
39. Ishida, K. & Nishizawa, T. The C-Co (Carbon-Cobalt) System. *J. Phase Equilib.* **12**, 417–424 (1991).
40. Tanaka, T., Ishihara, K. N. & Shingu, P. H. Formation of metastable phases of Ni-C and Co-C systems by mechanical alloying. *Metall. Trans. A* **23A**, 2431–2436 (1992).
41. Strelko, V. V. *et al*. Mechanism of reductive oxygen adsorption on active carbons with various surface chemistry. *Surf. Sci.* **548**, 281–290 (2004).
42. Palaniselvam, T., Biswal, B. P., Banerjee, R. & Kurungot, S. Zeolitic Imidazolate Framework (ZIF)-derived, hollow-core, nitrogen-doped carbon nanostructures for oxygen-reduction reactions in PEFCs. *Chem. Eur. J.* **28**, 9335–9342 (2013).
43. Ferrandon, M. *et al*. Multi technique characterization of a polyaniline–iron–carbon oxygen reduction catalyst. *J. Phys. Chem. C* **116**, 16001–16013 (2012).
44. Ai, K. L., Liu, Y. L., Ruan, C. P., Lu, L. H. & Lu, G. Q. Sp^2 C-dominant N-doped carbon sub-micrometer spheres with a tunable size: A versatile platform for highly efficient oxygen-reduction catalysts. *Adv. Mater.* **25**, 998–1003 (2013).
45. Roche, I., Chaînet, E., Chatenet, M. & Vondrák, J. Carbon-supported manganese oxide nanoparticles as electrocatalysts for the oxygen reduction reaction (ORR) in alkaline medium: physical characterizations and ORR mechanism. *J. Phys. Chem. C* **111**, 1434–1443 (2007).
46. Bard, A. J. & Faulkner, L. R. Electrochemical Methods: Fundamentals and Applications, Wiley: New York, 2000.
47. Zhao, Y. L. *et al*. Hierarchical mesoporous perovskite $La_{0.5}Sr_{0.5}CoO_{2.91}$ nanowires with ultrahigh capacity for Li-air batteries. *Proc Natl Acad Sci U S A* **109**, 19569–19574 (2012).
48. Wang, H. J., Ishihara, S., Ariga, K. & Yamauchi, Y. All-metal layer-by-layer films: bimetallic alternative layers with accessible mesopores for enhanced electrocatalysis. *J. Am. Chem. Soc.* **134**, 10819–10821 (2012).
49. Chen, S. G. *et al*. Nanostructured polyaniline-decorated Pt/C@PANI core–shell catalyst with enhanced durability and activity. *J. Am. Chem. Soc.* **134**, 13252–13255 (2012).

Acknowledgments

This study was supported by the National 973 (2011CB935900 and 2010CB631300), NSFC (21322101, 51101089, and 51371100), 863 (2012AA051503 and 2012AA051901), and 111 Project (B12015).

Author contributions

J.D., S.W. and T.Z. synthesized the materials, performed the characterization, and carried out the electrochemical tests. All authors contributed to results analysis and manuscript preparation. F.C. and J.C. supervised and directed the study.

Additional information

Supplementary information accompanies this paper at http://www.nature.com/scientificreports

Competing financial interests: The authors declare no competing financial interests.

How to cite this article: Du, J., Cheng, F.Y., Wang, S.W., Zhang, T.R. & Chen, J. M(Salen)-derived Nitrogen-doped M/C (M = Fe, Co, Ni) Porous Nanocomposites for Electrocatalytic Oxygen Reduction. *Sci. Rep.* **4**, 4386; DOI:10.1038/srep04386 (2014).